Nuclear Materials and Energy 35 (2023) 101449

Contents lists available at ScienceDirect

Nuclear Materials and Energy

journal homepage: www.elsevier.com/locate/nme

Influence of thermal annealing and of the substrate on sputter-deposited thin films from EUROFER97 on tungsten

E. Pitthan [a], T.T. Tran [a], D. Moldarev [a], M. Rubel [a,b], D. Primetzhofer [a]

[a] Department of Physics and Astronomy, Ångström Laboratory, Uppsala University, Box 516, SE-751 20 Uppsala, Sweden
[b] Department of Fusion Plasma Physics, KTH Royal Institute of Technology, 10044, Stockholm, Teknikringen 31, Sweden

A B S T R A C T

The modification of sputter-deposited films from EUROFER97 on tungsten during and after annealing were investigated in-situ and ex-situ. The annealing resulted in a densification of the film, formation of large grains, segregation of W at the surface, and the formation of Fe-W compounds at the interfacial region. Similar structural modifications were observed also for a film annealed on a MgO substrate, with an exception to the change in composition (no increase of W concentration). Results indicate that the substrate significantly affects thermally induced modifications of re-deposited EUROFER97.

Introduction

EUROFER97, a reduced activation ferritic-martensitic (RAFM) steel, was designed to be used for first wall and breeding blanket structural material in a future nuclear fusion reactor. In a demonstration power plant (DEMO), tungsten-coated EUROFER97 is intended to be used for plasma-facing components (PFC) [1]. Due to technical and economic advantages, uncoated RAFM steel is also considered for PFC in recessed areas of the reactor first-wall [2]. The plasma impact will result in the alteration of wall components by material migration processes comprising erosion and re-deposition accompanied by co-deposition of species eroded from the wall together with fuel atoms [3]. In this context, several studies have been conducted to determine the modifications of EUROFER97 by processes that will take place under the exposure to plasma: material migration, heat loads, and neutron and ion irradiation [4–8]. Experimental works are carried out to facilitate predictions of properties, especially potential deviation from the bulk counterpart. Recent studies of material properties and deuterium retention in sputter-deposited thin films from EUROFER97 [9] have shown similarities in the composition of the sputtered films and the bulk material. Despite that fact, the films presented lower density, significantly differences in microstructure (columnar structure and smaller crystallites) and higher hardness in comparison to the bulk. In real fusion devices re-deposited material will accumulate on different parts of the wall and, will be continuously subjected to modifications. Therefore, studies of re-deposited material and its behavior on different surfaces and under different environmental conditions will improve insight into the surface morphology of PFC in future reactors.

The aim of this work was to determine the changes induced in sputtered films from EUROFER97 by thermal annealing on different substrates. Special focus was given to tungsten (W) as substrate, since this is the main candidate for PFC due to its high melting temperature and low sputtering yield [10]. To investigate possible effects of the substrate impact on the film properties, in a series of comparative experiments a magnesium oxide (MgO) substrate was used. The modifications during annealing of the deposited film on W were monitored in-situ by ion beam analysis and ex-situ after the annealing by a combination of different techniques to evaluate the composition and microstructure.

Materials and methods

The entire experimental programme was accomplished at the Uppsala University: film production by sputtering, annealing of deposits and ion beam analysis at the Tandem Laboratory [11], while microscopy images were obtained at the Myfab Laboratory. Films were deposited in an argon atmosphere at a pressure of 0.55 Pa using a PREVAC magnetron sputtering system equipped with two MS2 63C1 Magnetron sources suitable for targets with 50.8 mm (2 in.) diameter and 1–6 mm thickness. A 1 mm thick target was cut from a EUROFER97-3 (ID 46) block. The composition of the films was previously determined by a set of complementary ion beam analysis (IBA), that resulted in atomic composition of 11% Cr, 88.7% Fe, and 0.3% W, being in good agreement with the nominal composition of the main components of EUROFER97 bulk: 9.5% Cr, 88.9% Fe, and 0.33% W [9]. Sputtered films were deposited with no intentional heating of the substrate for 160 min on W foil (99.9% nominal purity) initially cleaned in isopropanol, and on magnesium oxide (MgO (100) with $R_a < 0.5$ nm) to investigate the

E-mail address: eduardo.pitthan@physics.uu.se (E. Pitthan).

https://doi.org/10.1016/j.nme.2023.101449
Received 24 February 2023; Received in revised form 28 April 2023; Accepted 17 May 2023
Available online 22 May 2023
2352-1791/© 2023 The Author(s). Published by Elsevier Ltd. This is an open access article under the CC BY license (http://creativecommons.org/licenses/by/4.0/).

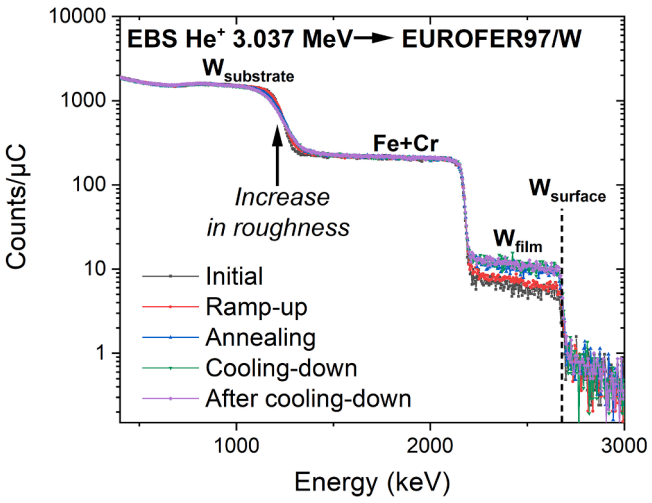

Fig. 1. EBS spectra employing 3.037 MeV He^+ primary ions and recorded in-situ for a sputter-deposited film from EUROFER97 on W during the indicated stages of the thermal annealing to 900 °C. The arrow indicates the interfacial region between film and substrate.

influence of the substrate. The resulted samples are named EUROFER97/W, and EUROFER97/MgO in this work, for simplification. MgO was chose as substrate for comparison to W due to its high thermal stability and chemical inertness. This way, undesired reactions between film and substrate are avoided [12]. More details of the deposition process and characterization of the films before annealing can be found in [9].

The annealing was performed in the SIGMA (Set-up for In-situ Growth, Material modification and Analysis) apparatus described in detail in [13]. This set-up allows for annealing with an e^--beam heating system under ultra-high vacuum (UHV) conditions and, further in-situ investigations with various IBA using a 5-MV NEC-5SDH-2 tandem accelerator (more details in [11]). Elastic and Rutherford Backscattering Spectrometry (EBS and RBS, respectively), Particle-Induced X-Ray Emission (PIXE), and Elastic Recoil Detection Analysis (ERDA) [4,14,15] were applied. The composition of the sample on W was monitored in-situ during annealing by EBS and PIXE simultaneously using a He^+ primary beam at 3.037 MeV. In EBS, a 30° incident angle with respect to the surface normal, with the detector placed at a scattering angle of 170° (solid angle of 2.08×10^{-3} sr, covered with a foil of ~139 nm Au and 44 nm C) and employing the narrow (≈10 keV) elastic resonance of ^{16}O $(\alpha,\alpha_0)^{16}O$ at 3.037 MeV [16] was used. The base pressure was ~ 10^{-8} mbar before/after the annealing and ~ 10^{-7} mbar during the annealing. The temperature was monitored using a pyrometer Optris CT 3 M positioned outside the chamber and focused in the center of the sample by a set of lasers. The heating rate was approximately 0.5 °C/s until the final temperature was reached. The direct heat from the e^--beam was applied on an area of 4 mm in diameter in the center of the sample, resulting in a temperature gradient outside this area that was used later to study the modifications induced by annealing at lower temperatures. The final temperature (900 °C) in the center was determined by averaging the temperature from the pyrometer with the one obtained by comparison to standard forging colors [an example can be observed in ref. [17], page 22], while the temperatures outside this area were assessed only by comparison to the standard forging colors. This approach allows to access the temperature of the sample in all regions independently of the pyrometer measurement. The annealing at 900 °C was carried out for around 1 h followed by a cool-down with a rate of approximately −2°C/s. The area of the sample that was not directly exposed to the e^--beam heating, and therefore was at a lower temperature (650 °C), was later analyzed separately. A similar procedure with a final temperature variation within 30 °C was repeated for the EUROFER97/MgO sample. After annealing, the films were also analyzed ex-situ in a different IBA set-up. RBS and PIXE with a beam of 2 MeV He^+ primary ions were performed simultaneously using a passivated implanted planar silicon (PIPS) detector (scattering angle of 170°), and a silicon drift detector (SDD), respectively. The fits to RBS spectra were performed using the SIMNRA code [18]. Time-of-flight elastic recoil detection analysis (ToF-ERDA) was also carried out ex-situ with a primary beam of 36 MeV $^{127}I^{8+}$ (details are described elsewhere [19]). Data evaluation and depth profiles were obtained employing the CONTES code [20].

For the characterization of the morphology and the crystal structure of the sample, electron microscopy techniques, including scanning electron microscopy (SEM) for analysis of the surface, scanning transmission electron microscopy (STEM) for analysis of the cross-section of the sample were employed. X-ray diffraction (XRD) was conducted for analysis of the crystal structure. Both SEM and STEM were accompanied with suitable Energy-dispersive X-ray Spectroscopy (EDX) for additional characterization of the film composition. For the EDX-SEM, a high-resolution Zeiss Crossbeam 550 SEM/FIB system was used, together with an Oxford Instruments AZtec EDS detector. This same system was also later used for preparing the cross-sectioned ultra-thin lamellae for the STEM analysis. A finely focused gallium ion beams was directed to

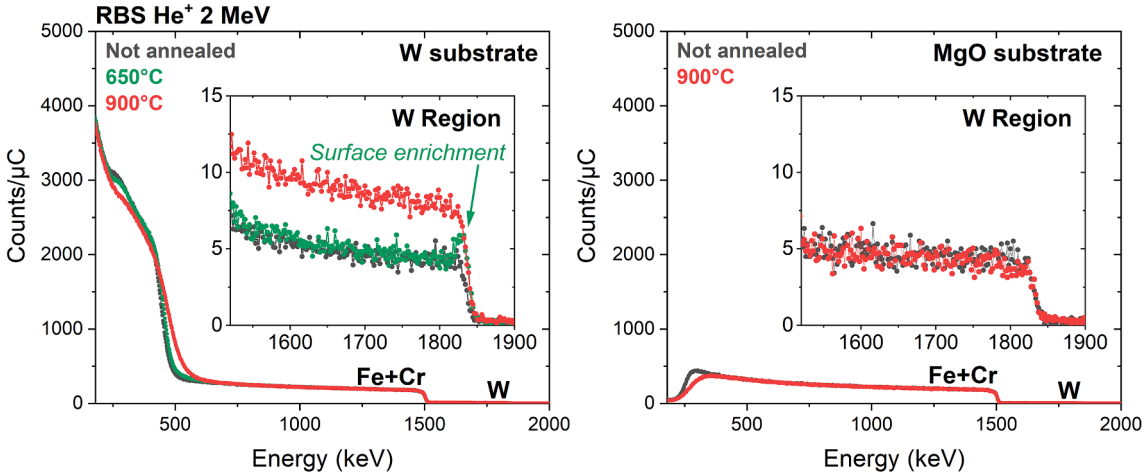

Fig. 2. RBS spectra, using 2 MeV He^+ primary ions, from sputter-deposited films for EUROFER97 on W (left) and MgO (right) as-deposited and after annealing. Insets: magnification of the region corresponding to scattering from W from the film. Arrow indicate the surface peak of W from the film. Normalization was performed using the signal from Fe + Cr target located close to the surface.

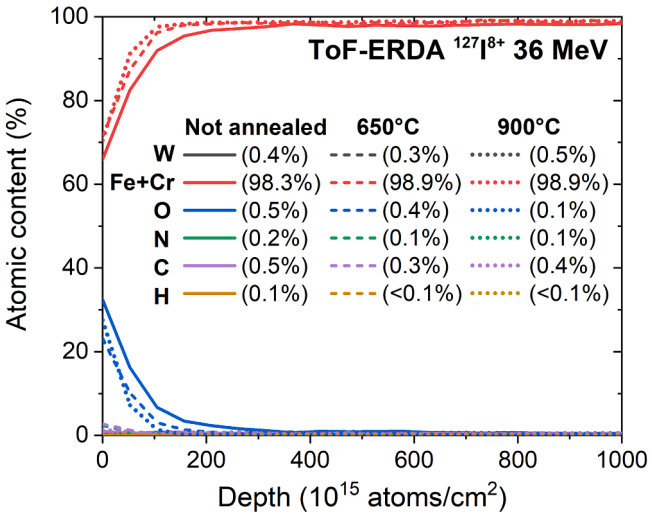

Fig. 3. Composition depth profiles for a deposited film from EUROFER97 on MgO (not annealed) and W (annealed) obtained using ToF-ERDA. The average atomic contents presented as inset are obtained in the depth interval from 1000 to 1500 $\times$ 10^{15} atoms/cm^2.

sculpt the lamellae out of the sample, which was then transferred from the sample to a TEM copper grid. The subsequent TEM was done with a FEI Titan Themis 200 STEM system equipped with a SuperX EDS instrument. The TEM was operated at an acceleration voltage of 200 kV. XRD was performed using a PANalytical Empyrean apparatus with Cu-Kα radiation. The incident angle was 10° to increase surface sensitivity and scans were carried out in steps of 0.02° (1 s per step) for 2θ ranging from 40° to 80°.

Results and discussion

The EBS spectra obtained in-situ before and during the annealing, and then during cool-down and after cooling-down for the film on a W substrate is presented in Fig. 1. The energy indicated as "W surface" is obtained from the kinematic factor and the energy loss of backscattered particles in the foil in front of the detector. Energies lower than that correspond to W deeper in the sample. No clear evidences of W surface enrichment were observed in the sample due to the high temperature used in accordance with earlier observations [6,7]. On the other hand, an overall increase in the W concentration in the film within probing depth (around 350 nm considering the energy from which on the W signal from the film overlaps with the much stronger Fe signal) is observed. This increase starts during the annealing rump-up (from 0.3 to 0.4 at. % of W), and stabilizes during annealing at 0.6 at. %. This value remains later unchanged during and after cooling-down. In addition, a continuous increase in roughness can also be observed during annealing, reaching its maximum and stabilizing during the cool-down (from SIMNRA simulations, full width at half maximum of thickness distribution in the film is increased from 400 (before annealing) to 880 $\times$ 10^{15} atoms/cm^2 (after cool-down)). A similar W enrichment was previously observed in the case of bulk EUROFER97 and it was attributed to the cooling of a sample annealed up to 1280 °C [6]. Phase transitions and

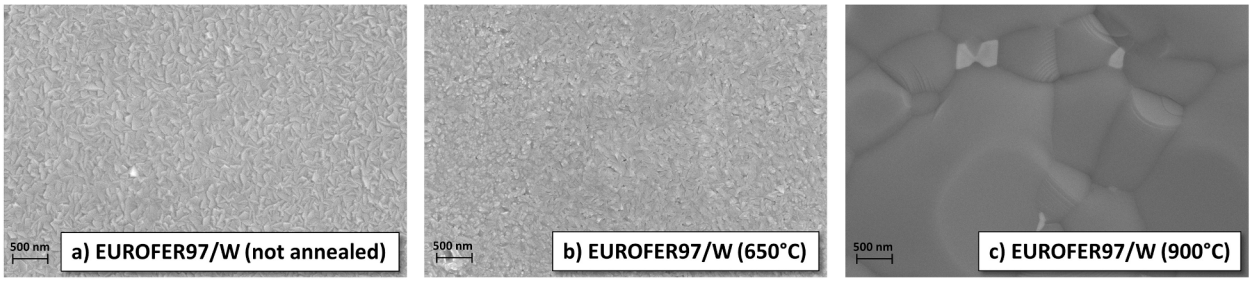

Fig. 4. SEM images of EUROFER97/W surfaces without (a) and after annealing (b and c). Formation of larger grains after annealing is observed in (c).

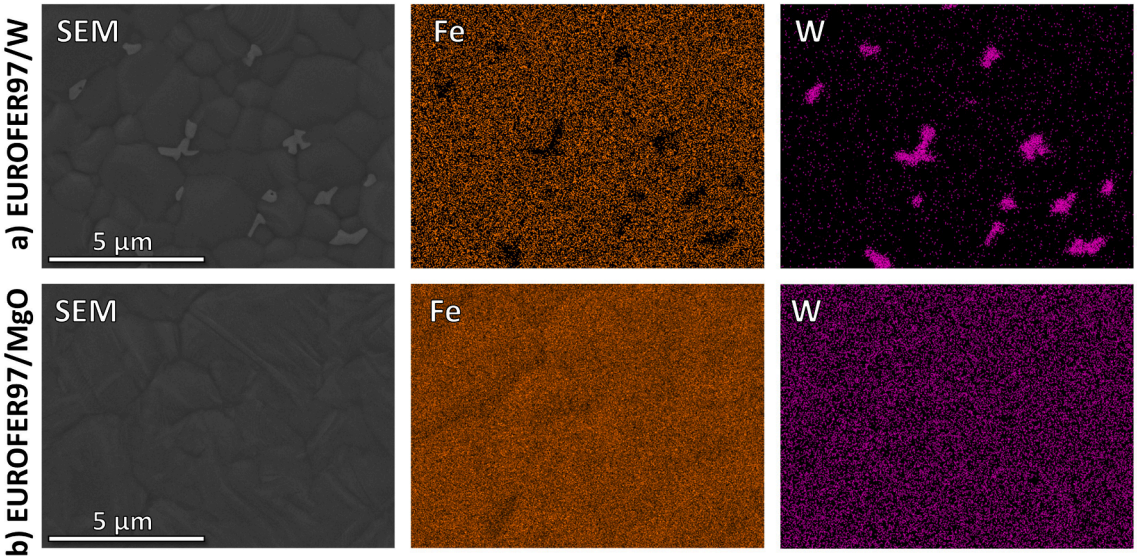

Fig. 5. SEM images (left column) and EDX elemental maps for Fe (center) and W (right) of sputter-deposited films from EUROFER97 on W (a) and MgO (b) substrates after annealing at 900 °C.

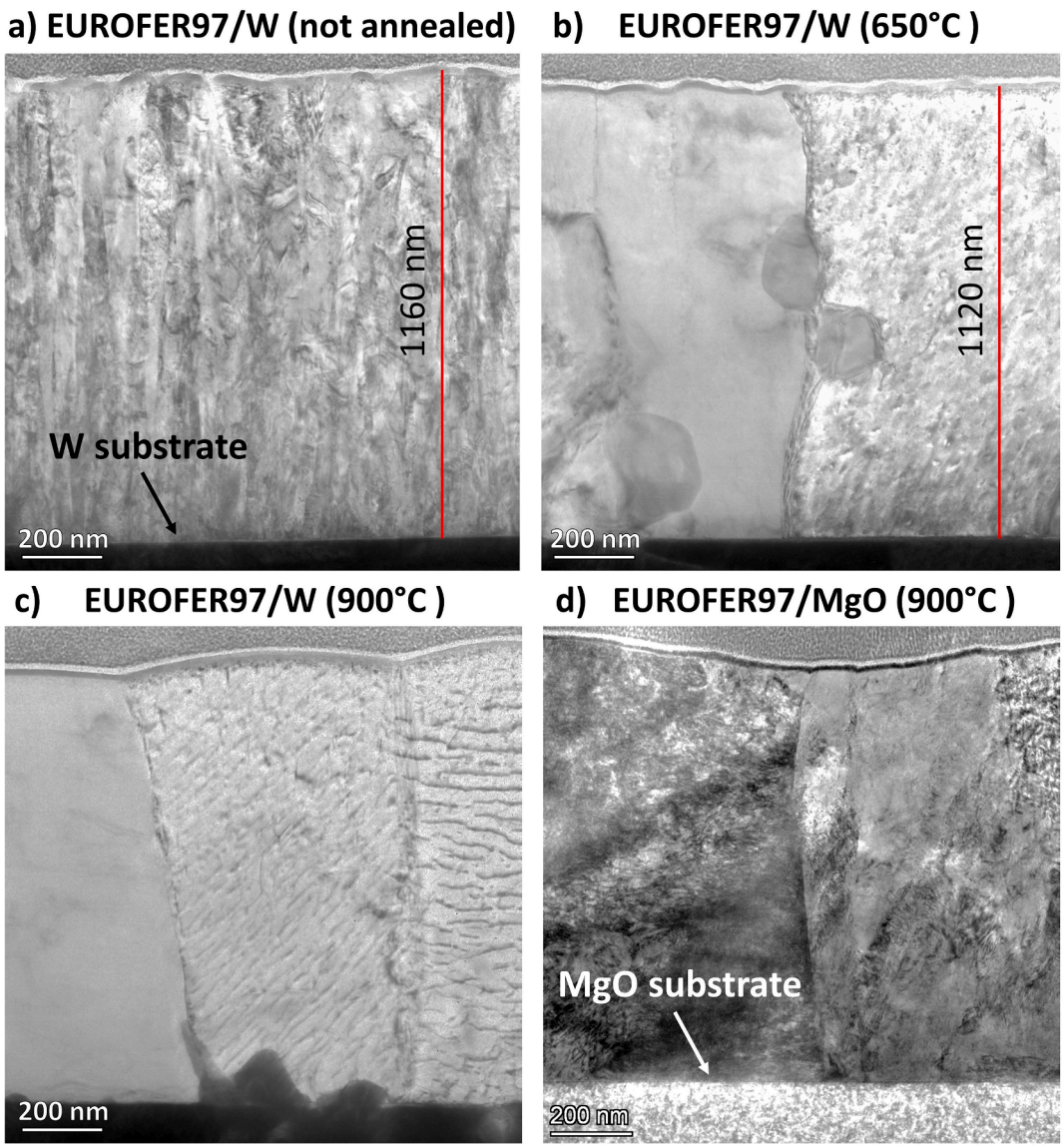

Fig. 6. TEM micrographs of cross sections of sputter-deposited films for EUROFER97 on W and MgO for pristine films and after annealing. The reduction of the film thickness from a) to b) indicate the densification of the film after annealing.

morphological changes due to the rapid cooling down were already observed in EUROFER97 bulk [21], and such modifications might be accompanied by a change of composition. In our case, we observed in-situ that both the increase of W concentration as well as morphological changes (increase in roughness) were already taking place during annealing, and not during/after cooling-down.

Ex-situ measurements were performed after annealing by RBS to compare the non-annealed samples (Fig. 2) to the annealed ones on the two different substrates. For the film deposited on tungsten, a surface enrichment with W can be observed for the region that was exposed to lower temperatures (650 °C), corresponding to an areal density of 0.54 $\times$ 10^{15} W atoms/cm^2. It agrees with previous findings in EUROFER97 bulk and Fe-W films around similar temperatures [6,7,22]. The increase of roughness after annealing is observed on both substrates, as indicated by the broadening of spectral features around the film/substrate interfacial region (energy range from 250 to 300 keV). In the case of the film annealed on a MgO substrate, no indications for a redistribution of W is observed within the accessible probing depth of the analysis (around 250 nm for this energy and geometry). These data confirm that the W as a substrate plays a significant role in the increase of W concentration in the film observed during annealing.

ToF-ERDA was performed to examine possible modifications in the composition and distribution of the light constituents in the film after the annealing. It was observed that films on W substrates before annealing are highly predisposed to delamination when subjected to the high energy iodine beam. A similar behavior was also observed for control films deposited on C substrates, while films on MgO and Si substrates were highly stable against higher currents and beams of energetic heavy ions. This higher stability is attributed to the higher surface energies of these substrates. Therefore, to avoid possible delamination, the annealed EUROFER97/W samples were measured with low current (6 nA) beam in comparison to a film deposited on a MgO substrate not annealed. From the depth profiles (Fig. 3), it is possible to observe that the annealing did neither directly nor indirectly led to the oxidation process by e.g. making the surface more receptive for oxygen (no increase of oxygen at. % in the surface region or in the bulk). In fact, the sample annealed at the highest temperature presents the lowest amount of oxygen both in the surface and in the bulk, indicating that the films were highly stable against oxidation. It is worth mentioning that loss of surface oxygen during annealing was observed for EUROFER97 bulk [6].

A comparison between surface morphology of the films deposited on

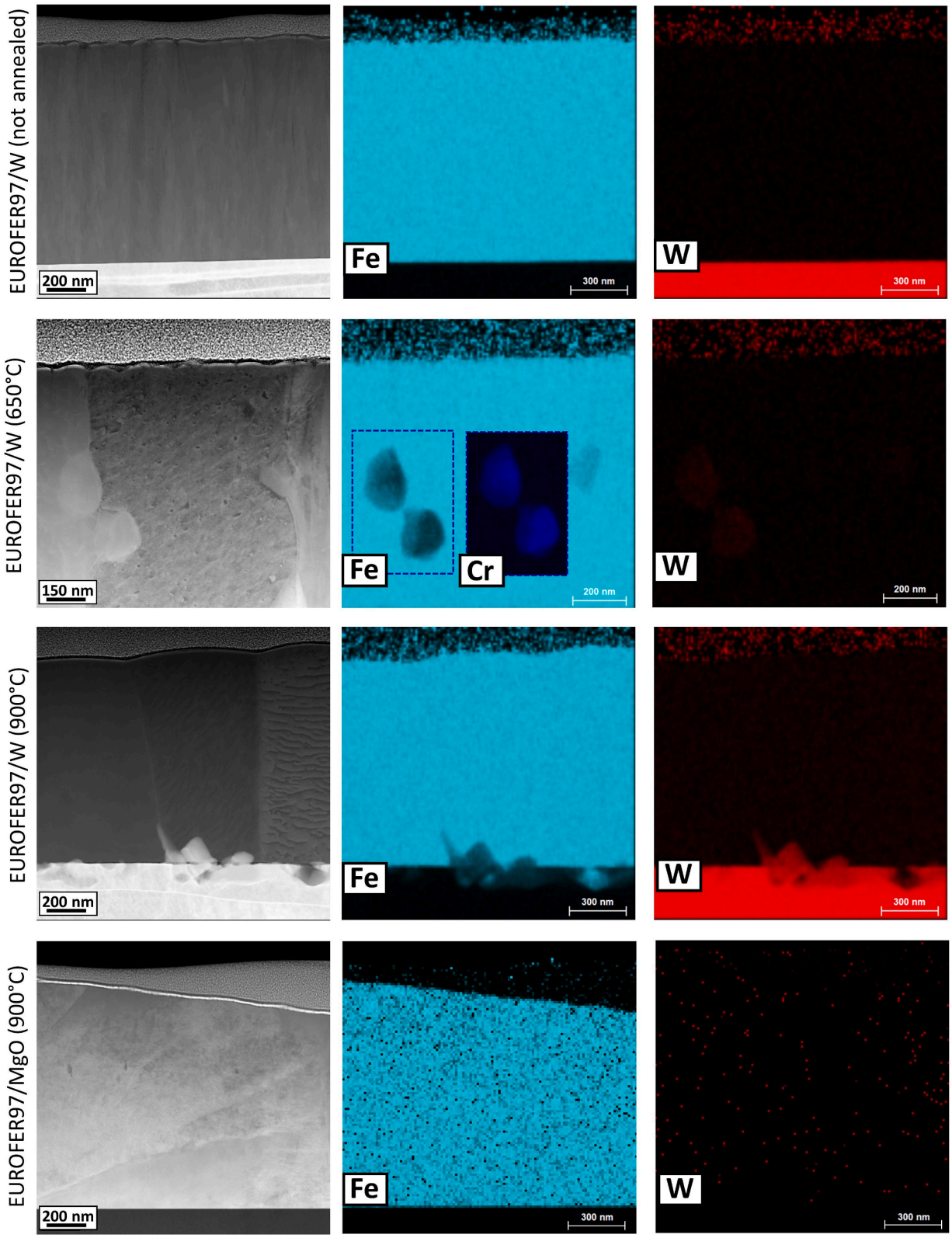

Fig 7. Cross-sectional STEM micrographs (left column), STEM-EDX elemental maps for sputter-deposited films from EUROFER97 on W and MgO not annealed and annealed.

W with and without annealing is possible from the SEM images presented in Fig. 4. The sample without annealing shows a surface morphology in agreement with a columnar microstructure [9]. After annealing at around 650 °C, a slight change in the surface morphology is noted by a reduction in roughness. After annealing at a higher temperature, significant modifications are evidenced by the formation of large crystal domains with width ranging from 300 to 3800 nm and well-defined boundaries.

The elemental mapping of the surfaces obtained by EDX is presented in Fig. 5 for films after annealing on both W and MgO substrates. The

formation of W precipitates in irregular shapes with width ranging from around 300 to 1300 nm is clearly observed for the surface of the film annealed on W substrate. These agglomerations with high W-concentration are in accordance with the increase in the concentration of W observed by RBS, considering that in the simulation of RBS spectra a homogeneous lateral distribution within the area of the beam spot (around 2 mm in diameter) is assumed. The presence of W enriched regions was confirmed by SEM to be homogeneously distributed in a larger area (86 × 114 μm) of the EUROFER97/W surface annealed at higher temperatures. EDX elemental maps also indicate a slight increase of carbon in the regions corresponding to the W enrichment, indicating the possible formation of carbides at the surface. A formation of large crystals is also observed in the film annealed on MgO (Fig. 5) but it is accompanied by a homogeneous distribution of W and Fe being also in agreement with the RBS spectra.

STEM cross-sections presented in Fig. 6 allow to evaluate modifications in film density, microstructure and surface/interfacial roughness after the annealing. The film on W substrate without annealing presents a thickness of 1160 nm and a columnar structure. A film density of 7.17 g/cm^2 is obtained using the areal density from RBS, that corresponds to 91% of the nominal density of the bulk. After annealing at 650 °C on W substrate, a densification of the film to 95% of the bulk density and the formation of large grains is observed. For the annealing at higher temperatures, large well-defined crystallites with well-defined boundaries are formed from the surface to the interface of the film for both W and MgO substrates. While the EUROFER97/MgO interfacial region after annealing presents a smooth interface, irregular agglomerations are observed within the EUROFER97/W interfacial region. Similar structures were observed along the entire interfacial region of the prepared lamella presented in Fig. 6c. XRD was also performed to evaluate possible modifications in the unit cell, stress in the structure, and potential phase changes. The lattice parameter was calculated using the (1 1 0) α-Fe peaks from the bcc polycrystalline structure without (2.873 ± 0.004 Å) and after annealing (2.874 ± 0.006 Å) for films on MgO. The absence of significant differences indicates that the crystal structure was not significantly affected by the annealing (i.e., no stress was introduced in the structure nor retained austenite after cooling), despite the significant differences in the microstructure observed by STEM.

The composition of the annealed and non-annealed films on different substrates analyzed by STEM images and EDX elemental maps are presented in Fig. 7. While quantitative analyses using EDX might present deviations in comparison to other methods such as IBA techniques, specially for low-Z species (see discussion in [23]), this technique is very helpful to access the elemental homogeneity and to estimate the stoichiometry of structures in the cross-sections of the prepared lamellas. While the film on W without annealing presents a homogeneous distribution of Fe and a well-defined interface with the W substrate in the analyzed region, it is possible to observe the presence of grains enriched in Cr and W in the region of the sample annealed at 650 °C. According to EDX, the composition of the grain is in average 47 at. % of Fe, 49 at. % of Cr, and 3 at. % of W balanced with V and S; while bulk values are 90 at. % of Fe, 8 at. % of Cr, and 1 at. % of W, also balanced with V and S. It is worth mentioning that precipitates enriched in C, V, Cr, and W are typically observed in EUROFER97 bulk structures formed due to manufacturing processes [4,24–26]. For the sample region annealed at a higher temperature, an interdiffusion between Fe from the film and W from the substrate is observed, given rise to Fe-W compounds in the interfacial region. From the quantitative EDX analysis, the composition of the Fe-W structure observed in the EUROFER97/W interfacial region is 61 at.% of Fe, and 29 at.% of W, corresponding approximately to Fe_2W. The interdiffusion of W and Fe and a formation of Fe-W phases agrees with Reisner et. al [27], that also observed the formation of Fe_2W at the interface between sputter-deposited W films on Fe after annealing at high temperatures (777–827 °C) for 12 to 48 h, while no Fe-W phase was observed for annealing at 627 °C. The increase of the total amount of W in the EUROFER97 film during annealing observed by IBA and formation of Fe-W compounds at the interfacial region is only possible given the presence of a W source from the W substrate.

Summary and conclusion

The composition and morphology of sputter-deposited films from EUROFER97 during and after annealing on different substrates (W and MgO) was investigated in-situ. The annealing resulted in significant transition of the film microstructure: from columnar to large grains formation. While no changes in the composition was observed for the annealed film on MgO, the EUROFER97/W structure resulted in segregation of W at the surface and the formation of Fe-W compounds at the interfacial region. The results indicate a significant impact of the W substrate during the annealing on the composition and microstructure of the film deposited by sputtering of EUROFER97. These presence of tungsten-rich regions at the surface of the film and the formation of Fe-W compounds at the interfacial region was only observed on the film annealed on a W substrate. Re-deposited EUROFER97 on W surfaces is likely to be formed at different locations in a reactor operated with W/EUROFER97 and uncoated EUROFER97 wall structures. Deposit modifications observed after thermal annealing are expected to be crucial for predicting consecutive erosion processes and dust formation during the reactor operation. The present work investigates the effects of annealing on EUROFER97/W layered systems in vacuum. Our results highlight the importance to investigate different combinations of structures that are likely to be formed in a reactor as well as their behavior under relevant conditions in the proximity of fusion plasmas. As the presence of hydrogen isotopes and/or contaminants such as oxygen, water vapor, or boron from wall conditioning could play a significant role in modifications of such structures, future studies investigating the behavior of similar systems in more complex environments are desirable.

CRediT authorship contribution statement

E. Pitthan: Conceptualization, Methodology, Investigation, Formal analysis, Visualization, Writing – original draft, Project administration. **T.T. Tran:** Investigation, Formal analysis, Visualization, Writing – review & editing. **D. Moldarev:** Investigation, Formal analysis, Writing – review & editing. **M. Rubel:** Conceptualization, Resources, Writing – review & editing, Supervision. **D. Primetzhofer:** Conceptualization, Resources, Writing – review & editing, Supervision, Project administration, Funding acquisition.

Declaration of Competing Interest

The authors declare that they have no known competing financial interests or personal relationships that could have appeared to influence the work reported in this paper.

Data availability

Data will be made available on request.

Acknowledgements

We are thankful to Petter Ström at Uppsala University for helpful discussions. This work has been carried out within the framework of the EUROfusion Consortium, funded by the European Union via the Euratom Research and Training Programme (Grant Agreement No 101052200 — EUROfusion). Views and opinions expressed are however those of the author(s) only and do not necessarily reflect those of the European Union or the European Commission. Neither the European Union nor the European Commission can be held responsible for them. Accelerator operation was supported by the Swedish Research Council VR-RFI, contracts #2019_00191.

References

[1] S. Brezinsek, et al., Plasma–wall interaction studies within the EUROfusion consortium: progress on plasma-facing components development and qualification, Nucl. Fusion 57 (2017), 116041.

[2] H. Bolt, V. Barabash, G. Federici, J. Linke, A. Loarte, J. Roth, K. Sato, Plasma facing and high heat flux materials – needs for ITER and beyond, J. Nucl. Mater. 307–311 (2002) 43–52.

[3] R.A. Pitts, J.P. Coad, D.P. Coster, G. Federici, W. Fundamenski, J. Horacek, K. Krieger, A. Kukushkin, J. Likonen, G.F. Matthews, M. Rubel, J.D. Strachan, JET.-EFDA. contributors, J D Strachan and JET-EFDA contributors, Material erosion and migration in tokamaks, Plasma Phys. Controlled Fusion 47 (12B) (2005) B303–B322.

[4] C. Dethloff, E. Gaganidze, J. Aktaa, Quantitative TEM analysis of precipitation and grain boundary segregation in neutron irradiated EUROFER97, J. Nucl. Mater. 454 (1-3) (2014) 323–331.

[5] R. Arredondo, M. Balden, A. Mutzke, U. von Toussaint, S. Elgeti, T. Höschen, K. Schlueter, M. Mayer, M. Oberkofler, W. Jacob, Impact of surface enrichment and morphology on sputtering of EUROFER by deuterium, Nucl. Mater. Energy 23 (2020), 100769.

[6] P. Ström, D. Primetzhofer, In-situ measurement of diffusion and surface segregation of W and Ta in bare and W-coated EUROFER97 during thermal annealing, Nucl. Mater. Energy 27 (2021), 100979.

[7] J. Shams-Latifi, P. Ström, E. Pitthan, D. Primetzhofer, An in-situ ToF-LEIS and AES study of near-surface modifications of the composition of EUROFER97 induced by thermal annealing, Nucl. Mater. Energy 30 (2022), 101139.

[8] M. Reinhart, S. Möller, A. Kreter, M. Rasinski, B. Kuhn, Influence of surface temperature, ion impact energy, and bulk tungsten content on the sputtering of steels: In situ observations from plasma exposure in PSI-2, Nucl. Mater. Energy 33 (2022), 101244.

[9] E. Pitthan, P. Petersson, T.T. Tran, D. Moldarev, R. Kaur, J. Shams-Latifi, P. Ström, M. Hans, M. Rubel, D. Primetzhofer, Thin films sputter-deposited from EUROFER97 in argon and deuterium atmosphere: Material properties and deuterium retention, Nucl. Mater. Energy 34 (2023) 101375.

[10] R. Neu, V. Bobkov, R. Dux, A. Kallenbach, Th. Pütterich, H. Greuner, O. Gruber, A. Herrmann, Ch. Hopf, K. Krieger, C.F. Maggi, H. Maier, M. Mayer, V. Rohde, K. Schmid, W. Suttrop, ASDEX Upgrade Team, Final steps to an all tungsten divertor tokamak 363–365 (2007) 52–59, https://doi.org/10.1016/j.jnucmat.2006.12.021.

[11] P. Ström, D. Primetzhofer, Ion beam tools for nondestructive in-situ and in-operando composition analysis and modification of materials at the Tandem Laboratory in Uppsala, J. Instrum. 17 (04) (2022) P04011.

[12] P. Ström, D. Primetzhofer, T. Schwarz-Selinger, K. Sugiyama, Compositional and morphological analysis of FeW films modified by sputtering and heating, Nucl. Mater. Energy 12 (2017) 471–477.

[13] K. Kantre, M. Moro, D. Moldaev, D. Johansson, D. Wessmann, M. Wolff, D. Primetzhofer, SIGMA: a set-up for in-situ growth, material modification and analysis by ion beams, Nucl. Instrum. Methods Phys. Res., Sect. B 463 (2020) 96–100.

[14] K. Kantre, P.S. Szabo, M.V. Moro, C. Cupak, R. Stadlmayr, L. Zendejas Medina, F. Aumayr, D. Primetzhofer, Combination of in-situ ion beam analysis and thermal desorption spectroscopy for studying deuterium implanted in tungsten, Phys. Scr. 96 (2021), 124004.

[15] C. Cupak, E. Pitthan, M.V. Moro, M. Fellinger, D. Primetzhofer, F. Aumayr, Retention of deuterium in beryllium: A combined investigation using TDS, ERDA and EBS, Nucl. Mater. Energy 33 (2022), 101249.

[16] J.A. Leavitt, L.C. McIntyre, M.D. Ashbaugh, J.G. Oder, Z. Lin, B. Dezfouly-Arjomandy, Cross sections for 170.5° backscattering of ^{4}He from oxygen for ^{4}He energies between 1.8 and 5.0 MeV, Nucl. Inst. Methods Phys. Res. B 44 (3) (1990) 260–265.

[17] T.G. Digges, S.J. Rosenberg, G.W. Geil, Heat treatment and properties of iron and steel, U.S. Government Printing Office (1960) 1–44.

[18] M. Mayer, SIMNRA, a simulation program for the analysis of NRA, RBS and ERDA, AIP Conference Proceedings 475 (1999) 541–544.

[19] P. Ström, P. Petersson, M. Rubel, G. Possnert, A combined segmented anode gas ionization chamber and time-of-flight detector for heavy ion elastic recoil detection analysis, Rev. Sci. Instrum. 87 (2016), 103303.

[20] M. Janson, CONTES conversion of time-energy spectra—A program for ERDA data analysis User manual, 2004.

[21] P. Ström, P. Petersson, R. Arredondo Parra, M. Oberkofler, T. Schwarz-Selinger, D. Primetzhofer, Sputtering of polished EUROFER97 steel: Surface structure modification and enrichment with tungsten and tantalum, J. Nucl. Mater. 508 (2018) 139–146.

[22] M. Mayer, T.F. Silva, R. Arredondo, M. Balden, I. Bogdanović-Radović, T. Höschen, H. Maier, M. Oberkofler, L. Ru, Z. Siketić, Tungsten surface enrichment in EUROFER and Fe-W model systems studied by high-resolution time-of-flight Rutherford backscattering spectroscopy, Nucl. Mater. Energy 17 (2018) 147–151.

[23] B. Bakhit, D. Primetzhofer, E. Pitthan, M.A. Sortica, E. Ntemou, J. Rosen, L. Hultman, I. Petrov, G. Greczynski, Systematic compositional analysis of sputterdeposited boron-containing thin films, J. Vac. Sci. Technol. A 39 (2021), 063408.

[24] P. Fernández, A.M. Lancha, J. Lapeña, M. Hernández-Mayoral, Metallurgical characterization of the reduced activation ferritic/martensitic steel Eurofer'97 on as-received condition, Fusion Eng. Des. 58–59 (2001) 787–792.

[25] M. Klimenkov, R. Lindau, E. Materna-Morris, A. Möslang, TEM characterization of precipitates in EUROFER 97, Prog. Nucl. Energy 57 (2012) 8–13.

[26] K. Wang, C.M. Parish, K.G. Field, L. Tan, Y. Katoh, Segregation behavior and phase instability of Eurofer97 after neutron irradiation to 72 dPa, J. Nucl. Mater. 547 (2021), 152834.

[27] M. Reisner, M. Oberkofler, S. Elgeti, M. Balden, T. Höschen, M. Mayer, T.F. Silva, Interdiffusion and phase formation at iron-tungsten interfaces, Nucl. Mater. Energy 19 (2019) 189–194.